Unravelling the characteristics of Al-alloy corrosion at the atomic to nanometre scale by transmission electron microscopy

Shravan K. Kairy[1,*], and *Nick* Birbilis[2]

[1]Department of Materials Science and Engineering, Monash University, Clayton, Victoria, 3800, Australia.
[2]College of Engineering and Computer Science, The Australian National University, Acton, ACT, 2601, Australia.

Abstract. The localised corrosion associated with Mg_2Si in the Al-matrix of an Al-Mg-Si alloy was studied in 0.1 M NaCl at pH 6 by quasi in-situ transmission electron microscopy. Herein, physical imaging of corrosion at the atomic to nanometre scale was performed. Phase transformation and subsequent chemical composition variations associated with the localised corrosion of Mg_2Si were studied. It was observed that corrosion initiated upon Mg_2Si, often preferentially at the interface with the Al-matrix, and propagated until Mg_2Si was completely dealloyed by Mg-dissolution, resulting in an amorphous SiO-rich phase remnant. The SiO-rich remnant became electrochemically inert and did not initiate corrosion in the Al-matrix. This study provides a clear understanding on the localised corrosion of Al-alloys associated with Mg_2Si. In addition, the methodology followed in this study can also be applied to understand the role of precipitates and second phase particles in the localised corrosion of Al-alloy systems.

1 Introduction

Precipitation hardenable aluminium (Al) alloys such as 6xxx (Al-Mg-Si-(Cu)), 2xxx (Al-Cu-(Mg)) and 7xxx (Al-Zn-Mg-(Cu)) are strengthened by alloying additions and heat treatment processes that cause evolution of nanoscale precipitates in the Al-matrix [1-2]. However, such microstructures, which are intentionally generated for increasing strength, notably deteriorate the localised corrosion resistance of the alloys [1-5]. Nanoscale precipitates exhibit electrochemical characteristics that are different from the Al-matrix, resulting in the selective dissolution of precipitates or the surrounding Al-matrix, leading to pitting and/or intergranular corrosion (IGC) [3-7]. The extent of localised corrosion experienced by different Al-alloys is dependent on the type (and composition) of precipitates within the alloy, and therefore, a definitive understanding of the role of specific nanoscale precipitates in the localised corrosion of Al-alloys is essential. Transmission electron microscopy (TEM) has the ability to image corrosion up to nanometre to atomic scale, and simultaneously record any chemical variations and phase transformations that occur during the corrosion process via energy dispersive X-ray spectroscopy (EDXS) and electron diffraction, respectively. Herein, as an example, the role of Mg_2Si in the localised corrosion of Al-alloys was studied using a quasi in-situ TEM technique [8].

Nanoscale Mg_2Si precipitates play a dominant role in increasing the strength of Cu-free 6xxx Al-alloys [1-2, 9-12]. However, these alloys suffer IGC with the evolution of Mg_2Si precipitates along grain boundaries during ageing [13-17]. Electrochemical tests were performed upon synthesised Mg_2Si bulk specimens, and also through the electrochemical microcell technique on microscale Mg_2Si particles in the Al-matrix [18-19]. Based on the tests, it was identified that Mg_2Si was less noble than the Al-matrix in neutral and acidic NaCl [18-19]. A consensus on the dealloying of Mg_2Si by Mg-dissolution in acidic and neutral NaCl exist [8, 18-39]. However, a consensus on the role of dealloyed Mg_2Si in the localised corrosion do not exist. Of the limited studies on Mg_2Si exist to date, a few studies reported that following complete dealloying of Mg_2Si by Mg dissolution, the Si-rich remnants were enriched in O and did not take part in the corrosion process [21-22, 30-33]. In contrast, ambivalent electrochemical characteristics of Mg_2Si in Al-alloys was also reported [34-38]. It was observed that following initial dealloying, MgSi remnants became cathodic, more noble than the Al-matrix, resulting in the dissolution of the Al-matrix [34-38].

Herein, the localised corrosion associated with an Mg_2Si particle in the Al-matrix of a 6xxx Al-alloy in 0.1 M NaCl at pH 6 was studied at nanometre to atomic scale by a quasi in-situ TEM technique.

* Corresponding author: shravan.kairy@monash.edu

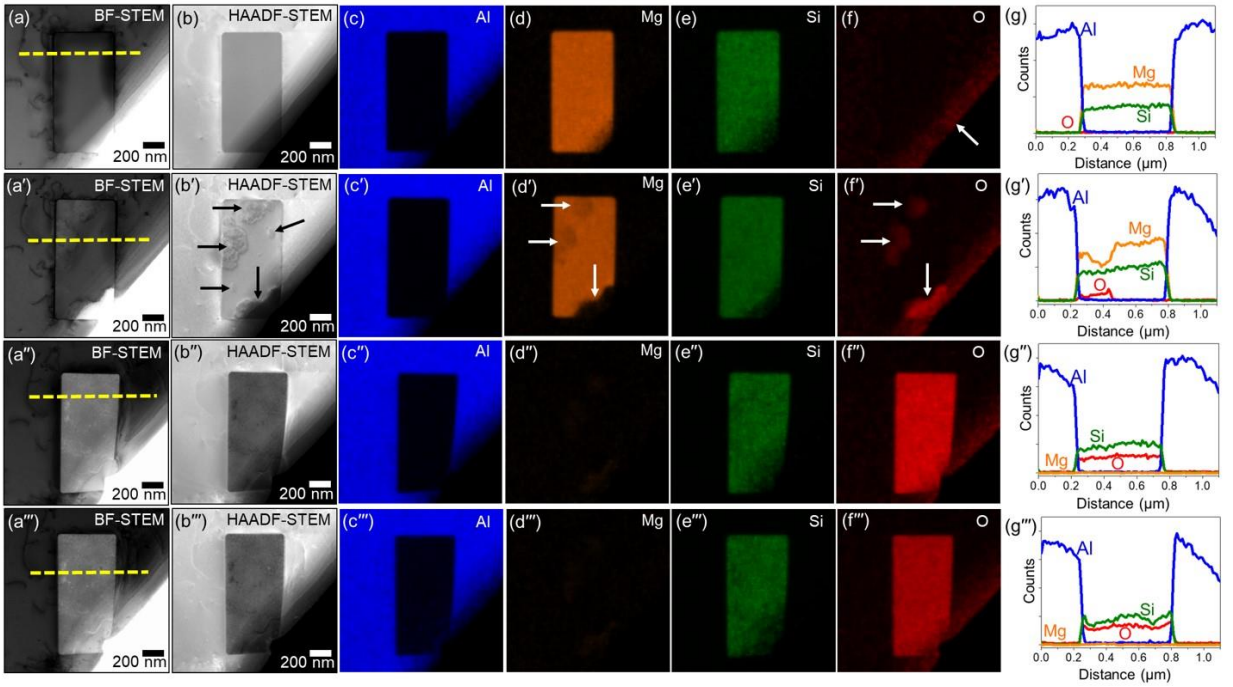

Fig. 1. BF- and HAADF-STEM images of an Mg_2Si particle in the Al-matrix of an Al-0.8Mg-0.6Si alloy, (a, b) prior to immersion, and following immersion in 0.1 M NaCl for (a′, b′) 3 s, (a″, b″) 30 s and (a‴, b‴) 30 min. Quantified EDXS maps in (c-f), (c′-f′), (c″-f″) and (c‴-f‴) correspond to (a, b), (a′, b′), (a″, b″) and (a‴, b‴), respectively. EDXS composition analysis along dashed lines in (a-a‴) are provided in (g-g‴), respectively. The arrow in (f) shows O enrichment in the Al-matrix at the edge of the TEM foil. Arrows in (b′) point to corroded sites within the Mg_2Si particle, and the Mg depletion and O enrichment at the corresponding sites are indicated by arrows in (d′) and (f′), respectively.

2 Experimental

2.1 Material

A 6xxx Al-alloy, Al-0.8Mg-0.6Si (% in mass fraction) was chosen for the present study. Alloy specimens were thermally treated in a PerkinElmer Pyris Diamond differential scanning calorimeter. The heat treatment involved solutionising at 540°C for 20 min and then cooling at 0.1 K/s to a room temperature. The detailed procedure was described elsewhere [40]. Such a thermal treatment resulted in the growth of monocrystalline Mg_2Si particles in the Al-matrix.

2.2 Transmission electron microscopy

A quasi in-situ TEM technique was applied to investigate the role of Mg_2Si in the localised corrosion of Al-alloys. Microstructural and microchemistry variations of an Mg_2Si particle in the Al-matrix were studied prior to immersion of a TEM specimen in 0.1 M NaCl at pH 6, and following immersion for 3 s, 30 s and 30 min. Specimens were subsequently cleaned in ethanol following immersion in NaCl, and vacuum dried prior to TEM observation.

A Gatan 691 precision ion polishing system was used for the TEM specimen preparation, which involved thinning of 3 mm diameter disc at - 80°C. In addition, a Gatan Solarus 950 advanced plasma system was used for plasma cleaning of TEM specimens for 2-10 min using an Ar and O_2 gas mixture, immediately prior to the specimen loading into a TEM. An FEI Tecnai G^2 F20 S-TWIN FEG TEM at 200 kV was operated in Scanning TEM (STEM) and TEM modes. In the STEM mode, bright field (BF) as well as high angle angular dark field (HAADF) images were collected. For microchemistry analysis, EDXS was performed with an X-flash X-ray detector using a Bruker Quantax 400. The collected EDXS hypermap data was then quantified by Cliff-Lorimer method using a Bruker Esprit1.9 X-ray software. In the TEM mode, electron diffraction to obtain selected area diffraction patterns (SADPs) and atomic resolution imaging were performed to study phase transformation associated with localised corrosion.

3 Results and Discussion

Scanning TEM imaging of an Mg_2Si particle in the Al-matrix and the corresponding chemical composition variations prior to and following a period of corrosion are provided in Fig. 1. In the pristine condition, i.e. prior to immersion in 0.1 M NaCl, a submicrometre sized Mg_2Si particle in the Al-matrix can be seen in Fig. 1 (a, b). The quantified chemical composition of the Mg_2Si particle and the surrounding Al-matrix as shown in Fig. 1 (c-f), revealed that the particle contained Mg and Si, with almost no O. The EDXS composition analysis over the dashed line in Fig. 1 (a) revealed that the particle contained higher Mg than Si, with negligible O content. The arrow in Fig. 1 (f) point to high O content in the Al-matrix, which is because of the sample preparation

technique and is quite common observation, at the edge of a TEM foil.

To understand the origin of corrosion, the TEM specimen was immersed in 0.1 M NaCl for a short period of 3 s and the same location as in Fig. 1 (a, b) was observed under TEM, and the results are shown in Fig. 1 (a′-g′). Arrows in Fig. 1 (b′) point to the sites at which corrosion occurred. It can be observed that corrosion initiated on the Mg_2Si particle mostly at the interface of the Mg_2Si particle and the Al-matrix, revealing that the Mg_2Si particle is anodic with respect to the Al-matrix (arrows in Fig. 1. (b′)). In addition, corrosion initiation sites were also observed upon the Mg_2Si particle away from the Mg_2Si particle and Al-matrix interface (arrows in Fig. 1. (b′)). The Mg_2Si particle dealloyed by Mg dissolution and subsequently enriched in O (arrows in Fig. 1 (d′ and f′)). The chemical composition analysis along the dashed line in Fig. 1 (a′) clearly revealed the dissolution of Mg and enrichment of O, with negligible change in Si, at the sites where the Mg_2Si particle corroded. Further immersion in 0.1 M NaCl for 30 s led to complete dissolution of Mg from the Mg_2Si particle and the remnant was enriched in O, with negligible change in Si (Fig. 1 (a″-g″)). To further investigate the role of the SiO-rich remnant on the corrosion, the TEM foil was further immersed for an extended period of 30 min in 0.1 M NaCl. It was revealed that following complete dissolution of Mg from the Mg_2Si particle, the SiO-rich remnant became electrochemically inert and did not take part in the corrosion process, as evident from the negligible change in the chemical composition within the dealloyed Mg_2Si particle and the surrounding Al-matrix, following 30 s and 30 min (Fig. 1 (a″-g″) and (a‴-g‴)).

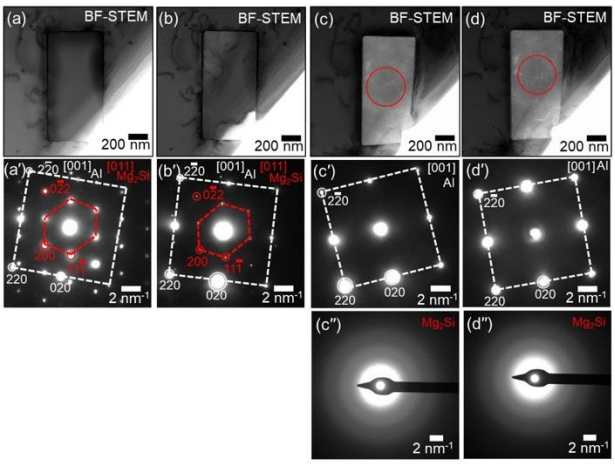

Fig. 2. BF-STEM images of the same Mg_2Si particle in the Al-matrix as shown in Fig. 1, (a) prior to immersion, and following immersion in 0.1 M NaCl for (b) 3 s, (c) 30 s and (d) 30 min. (a′-d′) are SADPs corresponding to (a-d), respectively. SADPs in (c″) and (d″) are collected from the region within the circles in (c) and (d), respectively.

To understand the phase transformation involved with the dealloying of the Mg_2Si particle following immersion in 0.1 M NaCl, electron diffraction studies were performed on the same Mg_2Si particle as shown in Fig. 1., prior to and following immersion, and the results are shown in Fig. 2. In the pristine condition, it was revealed that the orientation relationship of the Mg_2Si particle with the Al-matrix was $[001]_{Al}$ // $[011]_{Mg2Si}$ and $(1\bar{1}0)_{Al}$ // $(0\bar{1}1)_{Mg2Si}$ (Fig. 2 (a′)). The SADP obtained from Fig. 2 (b), i.e. following 3 s immersion, did not reveal any significant change in the corrosion-induced phase transformation, i.e. change in the chemistry and/or crystallographic structure, as the extent of corrosion is very small. A significant change in the electron diffraction was observed following complete dealloying of the Mg_2Si particle, i.e. following 30 s and 30 min (Fig. 2). Based on the results, it is quite evident that the crystalline Mg_2Si particle transformed to amorphous SiO-rich remnant, following dealloying by Mg dissolution.

Atomic resolution TEM imaging was performed along the $[001]_{Al}$ // $[011]_{Mg2Si}$ direction to understand the onset of corrosion at atomic scale and any influence of the SiO-rich remnant on the surrounding Al-matrix, and the results are provided in Fig. 3. Such a resolution is essential because the electron diffraction and chemical composition analysis will not be able to reveal significant details when the extent of corrosion is at the atomic scale. In the pristine condition, clear atomic columns or lattice fringes of the Mg_2Si particle and the Al-matrix were observed (Fig. 3 (a)). Following immersion for 3 s (Fig. 3 (b)), the lattice structure within the Mg_2Si particle transformed to amorphous, which was revealed to be of SiO-rich phase from the chemical composition analysis (Fig. 1 (a′-g′)), and the lattice structure of the Al-matrix did not change. A key finding from the present study is that the corrosion did not initiate uniformly upon the Mg_2Si particle at its periphery (Fig. 2 and 3 (b)). In fact, corrosion initiated randomly at few of the interfaces of the Mg_2Si particle and the Al-matrix, and propagated to completely dealloy the Mg_2Si particle. The direction of corrosion propagation was marked by a single arrowed line in Fig. 3 (b, b′). It is evident that with the propagation of corrosion, the crystalline Mg_2Si structure transforms to amorphous SiO-rich phase (Fig. 3 (b′)). Following complete dealloying of the Mg_2Si particle, i.e., after 30 s and 30 min immersion, the lattice structure of the Al-matrix at the interface of the amorphous SiO-rich phase remained unaffected (Fig. 3 (c, d and d′)), revealing that the SiO-rich remnant became electrochemically inert and did not initiate corrosion in the Al-matrix even at the atomic scale. The electrochemical behaviour of Mg_2Si in Al-alloys following extended period of exposure to 0.1 M NaCl at different pH was provided elsewhere [41]. In that study, it was revealed that the physical dimensions of Mg_2Si phase decreased following complete dealloying at pH 2, resulting in the formation of a trench at the Al-matrix and SiO-rich phase [41]. However, such significant change in physical dimensions was not observed following complete dealloying of Mg_2Si phase at pH 6 [41].

The results obtained from the present study aid in understanding the localised corrosion, i.e. pitting and IGC, of Al-alloys associated with Mg_2Si particles and precipitates. Upon exposure to NaCl, corrosion initiates on Mg_2Si, randomly at the interface of Mg_2Si and the Al-matrix, and also away from the interface (dotted arrows in Fig. 4 (a)). Corrosion propagates to completely dealloy Mg_2Si, leaving amorphous SiO-rich remnant that will become electrochemically inactive. As a result, pitting

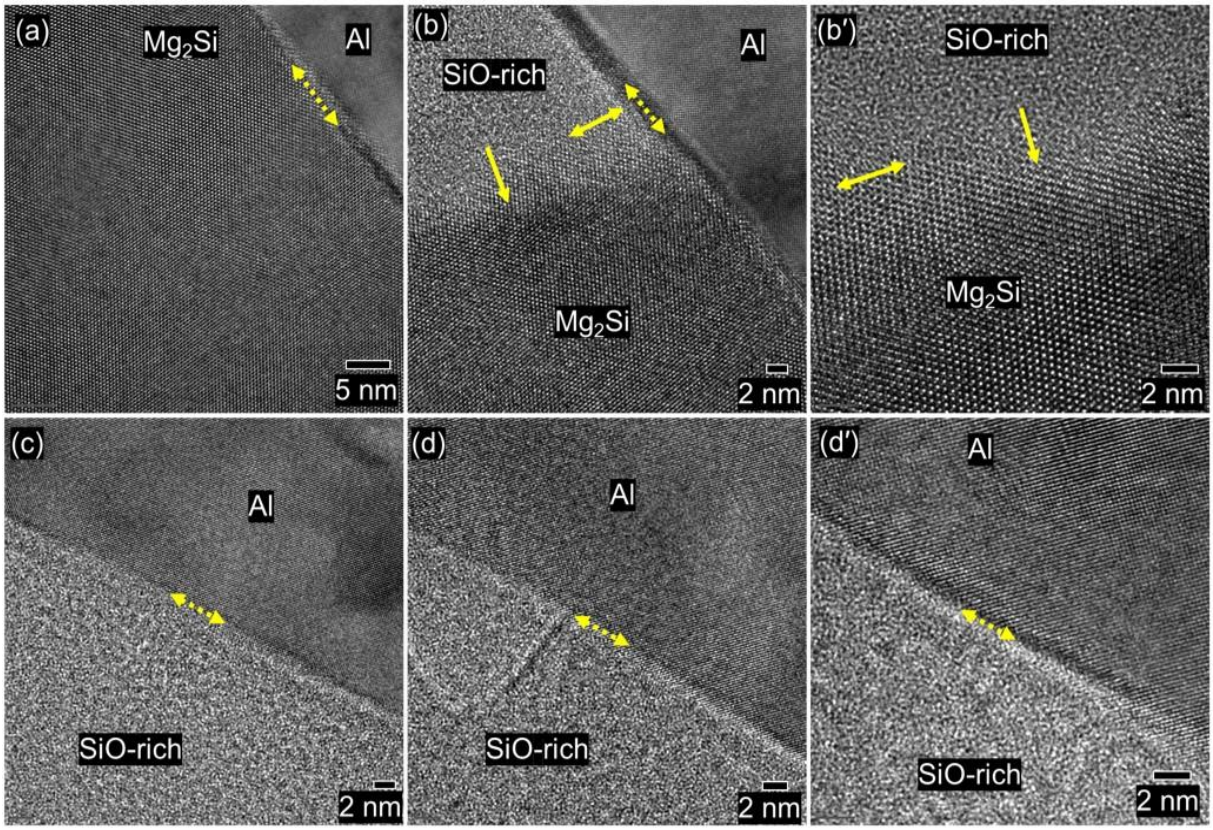

Fig. 3. Atomic resolution TEM images of an identical location showing Al-matrix, Mg_2Si and the interface between them, (a) prior to immersion, and following immersion in 0.1 M NaCl for (b) 3 s, (c) 30 s and (d) 30 min. (b′) shows atomic resolution Mg_2Si following immersion in 0.1 M NaCl for 3 s. (d′) shows higher magnification image of d. Double arrowed dotted lines in (a-d, d′) and solid lines in (b and b′) indicate interfaces between the phases. Whilst single arrowed solid line in (b) and (b′) indicate the direction of corrosion propagation.

will not be initiated within the Al-matrix following complete dealloying of Mg_2Si. Of the limited studies to date on IGC, a discrepancy exists in Cu-free alloys [14-17, 21-23, 42]. A few studies reported that upon artificial ageing, Cu-free 6xxx Al-alloys suffered IGC as result of the formation of Mg_2Si precipitates along grain boundaries [14-17, 42]. In contrast, these alloys were also reported to be immune to IGC though Mg_2Si precipitates form along grain boundaries [21-22]. From the present study, it can be understood that Mg_2Si precipitates along grain boundaries do not propagate IGC. However, the precipitates rapidly dealloy upon exposure during the IGC process, weakening grain boundaries. As a result, the propensity for IGC of Cu-free 6xxx Al-alloys depends on how closely the Mg_2Si precipitates are arranged along grain boundaries.

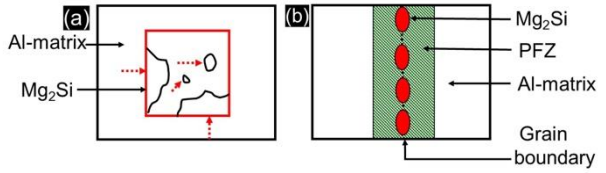

Fig. 4. Schematic microstructural model showing Mg_2Si (a) within the Al-matrix in a grain and (b) precipitates along a grain boundary. Dotted arrows in (a) point to corrosion initiation sites upon Mg_2Si. PFZ in (b) is a precipitate free zone, which is electrochemically more noble than Mg_2Si in 0.1 M NaCl at pH 6.

Conclusions

A quasi in-situ TEM method was employed to physically image corrosion initiation and propagation at the atomic to nanometre scale. The corresponding phase transformations (probed via electron diffraction) and chemical composition variations (probed via energy dispersive X-ray spectroscopy) that were associated with the localised corrosion of an Mg_2Si particle in the Al-matrix upon exposure to 0.1 M NaCl at pH 6 were studied. The following conclusions are drawn:

- Corrosion was initiated upon Mg_2Si either at its interface with the Al-matrix, but also was observed to initiate away from the interface with the Al-matrix.
- The corrosion process continued until the whole of Mg_2Si was completely dealloyed by Mg-dissolution, leaving an SiO-rich remnant.
- The SiO-rich remnant was determined herein to be amorphous and electrochemically inactive, and thus it did not take further part in, or initiate further, corrosion in the surrounding Al-matrix - even at the atomic scale.
- The research approach followed herein can be extended to other Al-alloy systems in understanding the corrosion phenomenon at nanometre to atomic scale.

Acknowledgements

The authors gratefully acknowledge P. Schumacher and B. Milkereit from University of Rostock, Germany, for the provision of the alloy. Microscopy was performed at the Monash Centre for Electron Microscopy (MCEM).

References

[1] I.J. Polmear, *Light alloys from traditional alloys to nanocrystals*, 4th ed. (Oxford, United Kingdom: Elsevier, 2006).
[2] J.F. Nie, "Physical metallurgy in light alloys", in *Physical metallurgy,* eds. D.E. Laughlin, K. Hono (Elsevier, Amsterdam, 2014).
[3] J.R. Davis, *Corrosion of aluminium and aluminium alloys*, 1st ed. (Materials Park: ASM International, 1999).
[4] S.K. Kairy, P.A. Rometsch, C.H.J. Davies, N. Birbilis, CORROSION **71**, 11 (2015) 1304-1307.
[5] S.K. Kairy, P.A. Rometsch, K. Diao, J.F. Nie, C.H.J. Davies, N. Birbilis, Electrochim. Acta **190** (2016) 92-103.
[6] S.K. Kairy, T. Alam, P.A. Rometsch, C.H.J. Davies, R. Banerjee, N. Birbilis, Metall. Mater. Trans. A **47**, 3 (2016) 985-989.
[7] S.K. Kairy, S. Turk, N. Birbilis, A. Shekhter, Corros. Sci. **143** (2018) 414-427.
[8] S.K. Kairy, P.A. Rometsch, C.H.J. Davies, N. Birbilis, CORROSION **73**, 1 (2017) 87-99.
[9] J.H. Chen, E. Costan, M.A. Van Huis, Q. Xu, H.W. Zandbergen, Science **312** (2006) 416-419.
[10] D.J. Chakrabarti, D.E. Laughlin, Prog. Mater. Sci. **49** (2004) 389-410.
[11] T. Saito, S. Muraishi, C.D. Marioara, S.J. Andersen, J. Royset, R. Holmestad, Metall. Mater. Trans. A **44** (2013) 4124-4135.
[12] A.K. Gupta, D.J. Lloyd, S.A. Court, Mater. Sci. Eng. A **316** (2001) 11-17.
[13] S.K. Kairy, P.A. Rometsch, C.H.J. Davies, N. Birbilis, CORROSION **73** (2017) 1280-1295.
[14] A. Laurino, E. Andrieu, J.P. Harouard, J. Lacaze, M.C. Lafont, G. Odemer, C. Blanc, J. Electrochem. Soc. 160 (2013) C569-C575.
[15] A. Laurino, E. Andrieu, J.P. Harouard, J. Lacaze, M.C. Lafont, G. Odemer, C. Blanc, ECS Trans. **41** (2012) 93-105.
[16] A. Shi, B.A. Shaw, E. Sikora, CORROSION **61** (2005) 534-547.
[17] A.K. Bhattamishra, K. Lal, Mater. Des. **18** (1997) 25-28.
[18] N. Birbilis, R.G. Buchheit, J. Electrochem. Soc. **152**, 4 (2005) B140-B151.
[19] R.K. Gupta, N.L. Sukiman, K.M. Fleming, M.A. Gibson, N. Birbilis, ECS Electrochem. Lett. **1**, 1 (2012) C1-C3.
[20] K.M. Fleming, A. Zhu, J.R. Scully, CORROSION **68** (2012) 1126-1145.
[21] M.H. Larsen, J.C. Walmsley, O. Lunder, K. Nisancioglu, J. Electrochem. Soc. **157** (2010) C61.
[22] G. Svenningsen, M.H. Larsen, J.H. Nordlien, K. Nisancioglu, Corros. Sci. **48** (2006) 3969-3987.
[23] W.J. Liang, P.A. Rometsch, L.F. Cao, N. Birbilis, Corros. Sci. **76** (2013) 119-128.
[24] J. Wloka, S. Virtanen, J. Electrochem. Soc. **154** (2007) C411-423.
[25] S. Jain, PhD Thesis, The Ohio State University, USA, 2006.
[26] C. Blanc, Y. Roques, G. Mankowski, Corros. Sci. **40** (1998) 1019-1035.
[27] O. Gharbi, N. Birbilis, J. Electrochem. Soc. **165** (2018) C497-C501.
[28] Y.T. Zhou, Y.N. Zan, X.X. Wei, B. Yang, B. Zhang, S.J. Zheng, X.H. Shao, J.H. Dong, X.K. Ma, B.L. Xiao, Q.Z. Wang, Z.Y. Ma, Corros. Sci. **153** (2019) 74-84.
[29] D.M. Sun, Y.M. Jiang, Q.W. Xiang, C. Zhong, J. Gong, L.H. Zhang, J. Li, Mater. Corr. **61** (2010) 105-110.
[30] K. Mizuno, A. Nylund, I. Olefjord, Corros. Sci. **43** (2001) 381-396.
[31] O. Knudsen, B.S. Tanem, A. Bjorgum, J. Mardalen, M. Hallenstvet, Corros. Sci. **46** (2004) 2081-2095.
[32] Y. Zhu, K. Sun, G.S. Frankel, J. Electrochem. Soc. **165** (2018) C807-820.
[33] K.A. Yasakau, M.L. Zheludkevich, S.V. Lamaka, M.G.S. Ferreira, Electrochim. Acta **52** (2007) 7651-7659.
[34] F. Eckermann, T. Suter, P.J. Uggowitzer, A. Afseth, P. Schmutz, Electrochim. Acta **54** (2008) 844-855.
[35] F. Zeng, Z. Wei, J. Li, X. Tan, Z. Zhang, Z. Zheng, Trans. Nonferrous Met. Soc. China **21** (2011) 2559-2567.
[36] Y. Wu, H. Liao, J. Mater. Sci. Technol. **29** (2013) 380-386.
[37] C. Li, J. Sun, Z. Li, Z. Gao, Y. Liu, L. Yu, H. Li, Mater. Charact. **122** (2016) 142-147.
[38] Z. Li, C. Li, Z. Gao, Y. Liu, X. Liu, Q. Guo, L. Yu, H. Li, Mater. Charact. **110** (2015) 170-174.
[39] L.L. Li, B. Zhang, B. Tian, Y. Zhou, J.Q. Wang, E.H. Han, W. Ke, J. Electrochem. Soc. **164** (2017) C240-C249.
[40] P. Schumacher, Ph.D. Thesis, University of Rostock, Germany, 2018.
[41] S.K. Kairy, N. Birbilis, CORROSION **76** (2020) 464-475.
[42] S.K. Kairy, P.A. Rometsch, C.H.J. Davies, N. Birbilis, CORROSION **73** (2017) 1280-1295.